NASA Contractor Report 187480
ICASE Report No. 90–83

ICASE

RESOLUTION OF THE 1D REGULARIZED BURGERS EQUATION USING A SPATIAL WAVELET APPROXIMATION

J. Liandrat
Ph. Tchamitchian

Contract No. NAS1–18605
December 1990

Institute for Computer Applications in Science and Engineering
NASA Langley Research Center
Hampton, Virginia 23665–5225

Operated by the Universities Space Research Association

National Aeronautics and
Space Administration

Langley Research Center
Hampton, Virginia 23665-5225

RESOLUTION OF THE 1D REGULARIZED BURGERS EQUATION USING A SPATIAL WAVELET APPROXIMATION

J. Liandrat[1]
IMST
12 avenue général Leclerc 13003 Marseille, France

Ph. Tchamitchian
CPT-CNRS Luminy
case 907-13288 Marseille, France
and
Faculté Saint Jérôme
Université Aix - Marseille III, Marseille, France

ABSTRACT

The Burgers equation with a small viscosity term, initial and periodic boundary conditions is resolved numerically using a spatial approximation constructed from an orthonormal basis of wavelets.

The algorithm is directly derived from the notions of multiresolution analysis and tree algorithms. Before the numerical algorithm is described these notions are first recalled. The method uses extensively the localization properties of the wavelets in the physical and Fourier spaces. Moreover, we take advantage of the fact that the involved linear operators have constant coefficients. Finally, the algorithm can be considered as a time marching version of the tree algorithm.

The most important point is that an adaptative version of the algorithm exists: it allows one to reduce in a significant way the number of degrees of freedom required for a good computation of the solution.

Numerical results and description of the different elements of the algorithm are provided in combination with different mathematical comments on the method and some comparison with more classical numerical algorithms.

[1]Research was supported in part by the National Aeronautics and Space Administration under NASA Contract No. NAS1-18605 while the author was in residence at the Institute for Computer Applications in Science and Engineering (ICASE), NASA Langley Research Center, Hampton, VA 23665 and also by AFOSR Grant No. 90-0093.

1. INTRODUCTION

The nonlinear parabolic equation

$$\frac{\partial u}{\partial t} + \frac{u \partial u}{\partial x} = \frac{\nu \partial^2 u}{\partial x^2} \tag{1}$$

known as the Burgers equation is one of the simplest combining both nonlinear propagation and diffusive effects. It represents a first step in the hierarchy of approximations of the Navier-Stokes equation. Solutions of this equation exhibit a delicate balance between the nonlinear advection and the diffusion terms. This situation leads to solutions with rapid and localized variations. Moreover, exact solutions are known (thanks to the Hopf-Cole transformation). Thus, this equation appears to be a very convenient and useful test problem for new numerical schemes.

This paper is devoted to the numerical resolution of the Burgers equation (1) with periodic boundary conditions on [0,1] and known initial condition: $u(0,t) = u(1,t); u(x,0) = \sin(2\pi x)$. We use a new algorithm based on a spatial approximation provided by an orthonormal wavelet basis exploiting as much as possible the numerical localization and regularity properties of the wavelets. One of the greatest advantages of this algorithm is that the whole method can automatically adapt itself to the generation of large gradient regions in the solution.

After a short review of the notions of multiresolution analysis and tree algorithms that are required for the construction of orthonormal wavelet bases and that are the keystones of our numerical algorithm, some properties of $r - regular$ wavelet bases and particularly of spline wavelets (Section 2) are recalled. The choices and definitions for the numerical algorithm are discussed first in the regular case (Section 3.1) and secondly in the adapted case (Section 3.2). Numerical results are presented in Section 4 with a complete description of the different elements of the method. Comparison with a classical Fourier pseudospectral method is provided. Section 5 is devoted to concluding remarks.

2. CONSTRUCTION AND BASIC PROPERTIES OF ORTHONORMAL WAVELET BASIS

The natural framework in which to construct bases of wavelets is given by the multiresolution analysis. This new concept, elaborated by S. Mallat and Y. Meyer, is also well adapted to the approximation of functions for numerical purposes.

The existence of a "Fast Wavelet Transform," based on the class of tree algorithms studied by S. Mallat and I. Daubeschies, is also a nodal point.

We briefly describe the main definitions and results we will need. The reader is referred to the book of Y. Meyer [Meyer 1987] for a complete account on the subject. Local analysis properties will demonstrate the quality of the wavelet approximation and help to explain the flagging process used in the adaptative version of the algorithm. The periodic spline wavelets will be presented at the end of this section and the different properties motivating their choice for the numerical resolution of partial differential equations will be recalled.

2.1. Multiresolution Analysis

As introduced by S. Mallat and Y. Meyer, a multiresolution of $L^2(\mathbb{R}^n)$ is a specific approximation scheme for finite energy functions. In this paper we restrict ourselves to $n = 1$. A multiresolution of $L^2(\mathbb{R})$ is an increasing sequence of closed linear subspaces $V_j, j \in \mathbb{Z}$ such that:

$$\bigcap_{-\infty}^{+\infty} V_j = \{0\}, \quad \bigcup_{-\infty}^{+\infty} V_j \text{ is dense in } L^2(\mathbb{R}) \tag{2.1}$$

$$f(x) \in V_j \Longleftrightarrow f(2x) \in V_{j+1} \tag{2.2}$$

$$f(x) \in V_0 \Longleftrightarrow f(x-k) \in V_0, \ \forall k \in \mathbb{Z} \tag{2.3}$$

(2.4) There exists a function $g(x)$ in V_0 such that the collection $g(x-k), k \in \mathbb{Z}$ is a Riez basis for V_0

(A collection of vectors $e_j, j \in J$, in a Hilbert space H is a Riez basis if any vector $x \in H$ can be written in a unique way as a sum $x = \sum a_j \, e_j$ where $(\sum |a_j|^2)^{1/2}$ is finite and defines an equivallent norm.)

The multiresolution analysis is called r-regular if the function $g(x)$ defined by (2.4) has the following property:

$$|\partial^\alpha g(x)| \leq C_p(1+|x|)^{-p} \text{ for } \alpha \leq r, \text{ all } x \in R \text{ and all integer } p. \tag{2.5}$$

This property can be interpreted as a quantification of the localization properties of the function g in the physical space ($\alpha = 0$) and in the Fourier space ($\alpha \geq 1$).

Let us give two examples of multiresolution analysis that generate classical spaces. The first one, to which people familiar with spectral methods automatically think, is provided by the Paley-Wiener analysis. In this analysis, V_j is made of functions whose spectrum belongs to the interval $[-2^{j-1}, 2^{j-1}]$. g is the cardinal sinus $g(x) = \frac{\sin(\pi x)}{\pi x}$. It is well-known that g

is infinitely derivable but is badly localized in the physical space. Consequently, for every value of r, this multi-resolution analysis is not r-regular.

The second example is the spline multiresolution which will provide the spline wavelets that will be used in the following numerical implementation of the algorithm . Here, given an integer $m \geq 2$, V_j consists of all functions with $m-2$ continuous derivatives whose restrictions to any interval $[k2^{-j}, (k+1)2^{-j}]$ coincide with a polynomial of degree less or equal to $m-1$. $g(x)$ is given by the so-called basic spline $g_m(x)$ which is the m fold convolution of the characteristic function of $[0,1]$. g_m is supported by $[0,m]$ and, satisfies (2.5) for $r = m-2$.

2.2. The Construction of Wavelets from the Multiresolution Analysis

The construction of the wavelet basis stems from the fact that during the process of refinement in the approximation one wants to only store the improvement from the approximation j to the approximation $j+1$. Mathematically, one introduces at each step j, the subspace W_j, defined as the orthogonal complement of V_j in V_{j+1}. The W_j space family satisfies the scaling (2.2) and translation invariance (2.3) properties imposed on V_j, so that attention can be focused on W_0. Then one has the fundamental theorem proved by S. Mallat and Y. Meyer.

Theorem: *There exists a function ψ of W_0 such that $\{\psi(x-k), k \in \mathbb{Z}\}$ is an orthonormal basis of W_0. ψ has the same regularity properties (2.5) as g, and ψ is an oscillating function:*

$$\int x^k \psi(x)dx = 0 \quad \text{for } 0 \leq k \leq r. \tag{2.6}$$

Then, the family of functions $\{\psi_{jk}(x) = 2^{j/2}\psi(2^j x - k), k \in \mathbb{Z}\}$ is an orthonormal family of W_j and, as $L^2(\mathbb{R}) = \oplus_{j \in \mathbb{Z}} W_j$, $\{\psi_{jk}(x), j \in \mathbb{Z}, k \in \mathbb{Z}\}$ is a hilbertian basis of $L^2(\mathbb{R})$. This family is an orthonormal wavelet family. Combined with (2.5) for $\alpha > 0$, equation (2.6) characterizes the localisation of the wavelet generating function in the Fourier space.

The proof of the theorem introduces an orthonormal basis of V_j that will be denoted by $\{\phi_{jk}(x) = 2^{j/2}\phi(2^j x - k), k \in \mathbb{Z}\}$. These functions are called by S. Mallat the scaling functions due to the fact that $\int \phi(x)dx = 1$. They satisfy the same regularity properties (2.5) as g.

Given an integer j_0 and writing $L^2(\mathbb{R}) = V_{j_0} \oplus \sum_{j \geq j_0} W_j$ one obtains another hilbertian basis of $L^2(\mathbb{R})$: $\{\phi_{j_0,k}, \psi_{jk}, j \geq j_0, k \in \mathbb{Z}\}$.

Let us go back now to the two examples:

The Paley-Wiener Analysis provides the wavelet generating function $\psi(x)$ given by:

$$\psi(x) = \frac{2}{\pi}\frac{\cos \pi x - \sin 2\pi x}{2x-1} \text{ and } \hat{\psi}(\omega) = e^{-i\pi\omega}\chi_{1/2 \leq |\omega| \leq 1}$$

where $\hat{\psi}$ stands for the Fourier transform of $\psi : \hat{\psi}(w) = \int \psi(x) e^{-2i\pi\omega x} dx$.

$\hat{\psi}$ has a compact support but the localization of ψ is poor as it decreases as $\frac{1}{|x|}$ at infinity and $\hat{\psi}(\omega) = 0$ if $|\omega| \leq \frac{1}{2}$, which means, in a weak sense, that all the moments of ψ are vanishing.

The spline multiresolution analysis provides the "exponentially localized wavelets" derived by P. G. Lemarié and G. Battle [Battle 1987, Lemarié 1989]. The generating wavelet $\psi(x)$ satisfies the following properties:

(2.7) $\psi(x)$ and all its derivatives to the order $m-2$ are continuous

(2.8) there exist $\varepsilon > 0$ such that $|\psi(x)| \leq C_0 e^{-\varepsilon|x|}, |\frac{\partial\psi}{\partial x}(x)| \leq C_1 e^{-\varepsilon|x|}, \cdots,$
$$|\frac{\partial^{m-2}\psi(x)}{\partial x^{m-2}}| \leq C_{m-2} e^{-\varepsilon|x|}$$

(2.9) $$\int_{-\infty}^{+\infty} x^k \psi(x) dx = 0 \text{ for } k = 0, \cdots, m-1$$

$\hat{\psi}$ is given in the Fourier space by

$$\hat{\psi}(w) = \frac{e^{-iw\pi}}{\left(\frac{\pi w}{2}\right)^m} \left[\frac{P_{m-1}\left(\cos^2 \frac{\pi w}{2}\right)}{P_{m-1}\left(\sin^2\left(\frac{\pi w}{2}\right)\right) P_{m-1}\left(\sin^2(\pi w)\right)} \right]^{\frac{1}{2}} \sin^{2m}\left(\frac{\pi w}{2}\right)$$

where P_m is the m order polynomial given by

$$\frac{P_{m-1}(\sin^2 w)}{(\sin w)^{2m}} = \sum_{k \in \mathbb{Z}} \frac{1}{(w + k\pi)^{2m}}.$$

The scaling function ϕ is also "exponentially localized" and satisfies:

$$\hat{\phi}(w) = \frac{1}{(\pi w)^m} \frac{\sin^m(\pi w)}{[P_{m-1}(\sin^2(\pi w))]^{\frac{1}{2}}}.$$

For $m = 6$ the generating spline wavelet ψ and scaling function ϕ are plotted in Figure 1.

2.3. Tree Algorithms

The tree or pyramidal algorithms are the basic tools for the fast computation of wavelet coefficients. Also, the numerical algorithm presented here is efficient thanks to its pyramidal structure.

If j_M is a given integer, fixing the level of approximation at 2^{-j_M}, the tree algorithm allows fast computation of the wavelet coefficients from $j_M - 1$ to an order $j_0, j_0 < j_M$, starting from the scaling coefficients in V_{j_M}.

Writing

$$V_{j_M} = V_{j_0} \oplus \sum_{j=j_0}^{j_M-1} W_j \tag{2.10}$$

and starting from the j_M approximation of a function U, we have

$$\Pi_{V_{j_M}}(U)(x) = \sum_{k \in \mathbb{Z}} 2^{j_M/2} c_{j_M,k} \phi(2^{j_M} x - k).$$

(Generally, Π_X stands for the orthogonal projector from $L^2(\mathbb{R})$ on the subspace X.) At each level j, S. Mallat [Mallat 1988] shows that, due to the orthogonality properties and the scaling, $\Pi_{W_{j-1}}(U)$ and $\Pi_{V_{j-1}}(U)$, written as:

$$\Pi_{W_{j-1}}(U)(x) = \sum_{\ell \in \mathbb{Z}} 2^{\frac{j-1}{2}} d_{j-1,\ell} \psi(2^{j-1} x - \ell)$$

and

$$\Pi_{V_{j-1}}(U)(x) = \sum_{\ell \in \mathbb{Z}} 2^{\frac{j-1}{2}} c_{j-1,\ell} \phi(2^{j-1} x - \ell)$$

can be computed from $\Pi_{V_j}(U)$ using the formulas:

$$d_{j-1,\ell} = \sum_k c_{j,k}\ g(2\ell - k)$$

and

$$c_{j-1,\ell} = \sum_k c_{j,k}\ h(2\ell - k)$$

where g and h are two discrete functions depending only on the multiresolution analysis and independent of j. These functions are precisely defined as:

$$\forall n \in \mathbb{N} : g(n) = \frac{1}{\sqrt{2}} < \psi_{-1,0}, \phi_{0,n} > \text{ and } h(n) = \frac{1}{\sqrt{2}} < \phi_{-1,0}, \phi_{0,n} >$$

with

$$g(-n) = g(n)\ ,\ h(-n) = h(n)$$

where $< .,. >$ stands for the $L^2(\mathbb{R})$ inner product ($< f, g >= \int f(x)g(x)dx$).

Practically, it means that with the storage of two discrete functions h and g which are well localized thanks to the localization of ψ and ϕ , one computes with an order of $N \text{Log} N (2^{j_M} = N)$ operations the $(2^{j_M} - 2^{j_0})$ wavelet coefficients and the 2^{j_0} scaling coefficients corresponding to the formula (2.10). The discrete functions $h(n)$ and $g(n)$ are plotted on Figure 2 in the

physical and Fourier spaces in the case of the spline multiresolution with $m = 6$. They classically appear as a low pass filter and a high pass filter respectively.

2.4. Approximation properties of Wavelets

Approximation properties of orthonormal wavelets can be interpreted from different points of view:

As the space generated by the wavelets up to an order $j-1$ is the space V_j of the multiresolution, the approximation results are driven by the properties of the scaling function $2^{j/2}\phi(2^j x)$ that, with its translates ϕ_{jk}, generate V_j. It is then a more classical problem of approximation by translates. The general results relating the quality of the approximation to the degree r of r-regularity of the multiresolution can be found in Y. Meyer's book [Meyer 1990].

Moreover, if the space V_j is split in the different contributions of $W_l, l \leq j-1$, a characterization of the Sobolev space $H^s(\mathbb{R})$ can be obtained from the decay of the wavelet coefficients as :

Theorem: *If f belongs to $H^{-r}(\mathbb{R})$, if $V_j, j \in \mathbb{Z}$ is a r-multiresolution of $L^2(\mathbb{R})$ and if $-r \leq s \leq r$ then f belongs to $H^s(\mathbb{R})$ if and only if $\Pi_{V_0}(f) \in L^2(\mathbb{R})$ and $||\Pi_{W_j}(f)||_2 = \varepsilon_j 2^{-js}, j \in \mathbb{N}$, where $\varepsilon_j \in l^2(\mathbb{N})$.*

Another important result for approximation by wavelets deals with the characterization of singularities from the wavelet decomposition. The singularity of a function at a point x_0 can be described with the Lipschitz exponent α defined as:

$f(x)$ is α Lipschitz at x_0 ,$(0 \leq \alpha \leq 1)$ if and only if for all x in a neighborhood of x_0 one has:

$$|f(x) - f(x_0)| = O(||x - x_0||^\alpha).$$

The following theorem holds:

Theorem: *A function f belonging to $L^2(\mathbb{R})$ is α Lipschitz with $0 \leq \alpha < 1$ in all points of an open interval if and only if for all x in the interval one has:*

$$| < f, \psi_{jk} > | = O(2^{-j(\alpha+1/2)}).$$

As pointed out by Stephane Mallat [Mallat 1990], an extension of this result can be obtained when the initially α singular function f is smoothed by a smoothing kernel. For instance with a gauusian of variance σ one has the following result:

The wavelet coefficient of the smoothed function at the scale 2^{-j} is of the same order of magnitude as the wavelet coefficient of the original function f at the scale $s = \sqrt{2^{-2j} + \sigma^2}$. The previous theorem then holds by changing 2^{-j} in $\sqrt{2^{-2j} + \sigma^2}$.

On one hand, when $2^{-j} \gg \sigma$, i.e., when the scales under study are larger than the smoothing scale, the previous theorem shows that the characterization of the degree α from the wavelet coefficients of the smoothed function is still possible. On the other hand, when $2^{-j} \ll \sigma$, the scaling effect disappears and no characterization of the degree of singularity is possible from the wavelet coefficients of the smoothed function.

2.5. Periodic Spline Wavelets

As pointed out by Y. Meyer [Meyer 1990], the complete tool box built in $L^2(\mathbb{R})$ can be used in the periodic case for $L^2([0,1])$ by introducing a standard periodization technique. It has been implemented by V. Perrier and C. Basdevant [Perrier and Basdevant 1989]. This technique consists at each scale in folding, around the integer values, the wavelets ψ_{jk} and the scaling functions ϕ_{jk} centered in $[0,1]$ resulting in

$$\psi p_{jk}(x) = \sum_{l \in \mathbb{Z}} \psi_{jk}(x - l)$$

and

$$\phi p_{jk}(x) = \sum_{l \in \mathbb{Z}} \phi_{jk}(x - l).$$

This folding provides a multiresolution analysis of $L^2([0,1])$. Due to the finite size of [0,1], j takes only positive values and k takes a finite number of values at each scale: $0 \leq k \leq 2^j - 1$. Moreover, the periodized function $\phi p_{0,0}$ that generates Vp_0 is constant and equal to 1. Following V. Perrier and C. Basdevant, the periodic m order spline scaling functions and wavelets are

$$\begin{cases} \hat{\phi p}_{j,0}(w) = \frac{1}{2^{j/2}} \hat{\phi}\left(\frac{w}{2^j}\right) \\ \hat{\psi p}_{j,0}(w) = \frac{1}{2^{j/2}} \hat{\psi}\left(\frac{w}{2^j}\right) \end{cases}$$

where ϕp_{jk} and ψp_{jk} generate respectively V_{pj} and W_{pj}.

For simplicity in the notation, from now on the subscript p will be removed. When necessary the subscript up will be added for the non periodized functions.

As far as numerical application is concerned, the spline multiresolution offers the following advantages.

First, it is known that if the degree m of the spline is even, there exists a Lagrangian interpolant function g_{j_M} of V_{j_M} such that $g_{jM}(k2^{-j_M}) = \delta_{k,0}$. ($\delta$ stands for the Kronecker symbol: $\delta_{k,0} = 1$ if and only if $k = 0$.) The functions $g_{j_M}(x - k2^{-j_M})$ $0 \leq k < 2^{j_M}$ are then

an unconditional basis of V_{j_M}. Thanks to this basis, it is possible, for any function $U(x)$, to consider its interpolation on V_{j_M} given by

$$\Pi_{cV_{j_M}}(U)(x) = \sum_{0 \leq k < 2^{j_M}} U(k2^{-j_M}) g_{j_M}(x - k2^{-j_M}).$$

This collocation projection is very useful when one wants to apply the classical but efficient pseudospectral treatment to nonlinear terms (see Section 3.1.5).

A second point of interest stems the numerical localization of the generating functions ψ_{up} and ϕ_{up} in physical and Fourier spaces. Numerically, the exponential decay of these functions can be described by the required support to which ψ_{up} or ϕ_{up} (or $\hat{\psi}_{up}$ and $\hat{\phi}_{up}$) can be restricted without altering their L_2 norms (equal to 1) up to a fixed precision α.

In the physical space, the support of the periodized functions ϕ_{jk} and ψ_{jk} is directly connected to the support of $\phi_{up\ jk}$ and $\psi_{up\ jk}$ as soon as the length of these last supports is less than 1 (otherwise the support of ϕ_{jk} and ψ_{jk} is $[0,1]$). Moreover if $S_{\phi_{up}}$ and $S_{\psi_{up}}$ are the supports of ϕ_{up} and ψ_{up} the supports of $\phi_{up\ jk}$ and $\psi_{up\ jk}$ are respectively $\frac{S_{\phi_{up}}}{2^j}$ and $\frac{S_{\psi_{up}}}{2^j}$. For $m = 6$, the following estimations are obtained:

precision α	support of ϕ_{up}	support of ψ_{up}
10^{-3}	$\lvert x \rvert < 3.50$	$\lvert x \rvert < 3.25$
10^{-4}	$\lvert x \rvert < 4.75$	$\lvert x \rvert < 4.75$

and an estimate of the increase of the length of these supports with m can be found in [Perrier and Basdevant 1989]. For $j \geq 3, m = 6$ and up to a precision $\alpha = 10^{-4}$, the functions $(\phi_{up})_{jk}$ and $(\psi_{up})_{jk}$ have a numerically compact support of length less than 1.

In the Fourier space, the periodization does not affect the support of the functions $\hat{\phi}$ and $\hat{\psi}$. If S_i are the bounds of the support of $\hat{\phi}$ (or $\hat{\psi}$), $2^j S_i$ are the bounds of the support of $\hat{\phi}_{jk}$ (or $\hat{\psi}_{jk}$). For $m = 6$ we obtained

precision α	support of $\hat{\phi}$	support of $\hat{\psi}$
10^{-3}	$\lvert w \rvert < 0.625$	$0.34 < \lvert w \rvert < 1.29$
10^{-4}	$\lvert w \rvert < 0.685$	$0.27 < \lvert w \rvert < 1.40$

The length of these supports decreases as m increases. We will strongly use the fact that, for $m = 6$ and $\alpha = 10^{-3}$, the numerical supports of $\hat{\psi}_{jk}$ and $\hat{\psi}_{j+2,k}$ are disconnected.

A third advantage of the spline wavelets is the very easy control of their cancellation (the first $m - 2$ moments of each wavelet vanish). As has been shown in Section 2.4, on one hand, this property is required to have a good convergence of the wavelet series and a

good characterization of the local properties of the analyzed function. On the other hand, as m increases the localization in the physical space of the wavelet decreases. To obtain a "satisfactorily localized function" with "good cancellation," one has to define a compromise for the choice of m. All the numerical results presented in this paper are obtained with $m = 6$.

To be complete, one must recall that an efficient implementation of periodic spline wavelet decomposition has been described by V. Perrier and C. Basdevant [Perrier et al. 1989]. It allows computation with order of $NLog(N)$ operations of the wavelet coefficients of a periodic function described by N regularly distributed collocation points. This algorithm has been extended to a non complete (non regular) distribution of points.

3. THE ALGORITHM

Taking apart the Lagrangian methods, numerical algorithms can be roughly speaking separated into three families: finite difference schemes, finite element methods and spectral schemes.

The class of finite difference schemes is known to be very efficient in intricate configurations because it can be easily adapted to resolve localized difficulties such as large gradient regions or sharp boundary conditions. This flexibility, however, hides a difficulty in controlling precision. Moreover, the computation cost increases considerably with the precision.

The finite element schemes offer a better controlled precision and are extensively used for intricate boundary condition problems in multidimension. However they suffer from difficulties in getting very flexible and fast algorithms.

The precision of spectral methods is well-known ([Gottlieb and Orszag 1977], [Canuto et al. 1987]) and their efficiency for problems with a high degree of regularity has been demonstrated. However, they are fundamentally ill-suited to problems that develop strong local gradients or discontinuities in their solutions.

The wavelet approach provides a multiscale decomposition based on orthonormal, regular and numerically well localized functions. It can then a priori offer an interesting compromise between precision, efficiency, and adaptability.

3.1. Description of the Algorithm on a Regular Grid

3.1.1. The Grid Points

Given a family of wavelets, one can characterize the space X that they generate by the dyadic grid built from the set of all $y_{jk} = \frac{k}{2^j} + \frac{1}{2^{j+1}}$ such that ψ_{jk} belongs to X (see Figure 3).

If X is a space V_{j_M}, then a regular grid corresponding to the centers of the scaling functions $\phi_{J_M k}$ is built from the x_k. 2^{j_M} is the level of approximation.

3.1.2. The Algorithm

The algorithm is first described generally for the evolution equation

$$(3.1) \qquad \begin{cases} \frac{\partial U}{\partial t} + LU + G(U) = 0 \\ U(0,t) = U(1,t) \\ U = U_0 \text{ for } t = 0 \\ t \geq 0, 0 \leq x \leq 1 \end{cases}$$

where L is a linear operator and G is a function of U and its derivatives. An approximate solution U_M, belonging to a trial space X_M, ($X_M = V_{j_M}$ in the case of a regular grid) is sought as a solution of the equation:

$$\begin{cases} \frac{\partial U_M}{\partial t} + L_M U_M = \Pi_{X_M}(G(U_M)) \\ U_M(x,0) = \Pi_{j_M} U_0. \end{cases}$$

Here L_M is an approximation of L, of the form $P_{X_M} L \Pi_{X_M}$, where Π_{X_M} is the orthogonal projection onto X_M, and P_{X_M} is another projection onto X_M parallel to the orthogonal of Y_M, another space to $\Pi_{X_M}(G(u_M))$; the approximate equation becomes

$$(3.2) \qquad \begin{cases} \frac{\partial U_M}{\partial t} + L_M U_M = G_M \\ U_M(x,0) = U_{0_M}(x). \end{cases}$$

Using the classical name conventions for the Methods of Weighted Residuals (MWR) (see [Canuto et al. 1987]), we call trial functions the wavelets $\psi_{jk}, 0 \leq j < j_M, 0 \leq k < 2^j$ and $\phi_{0,0}$ and introduce a family of functions $\theta_\tau, \tau \in T$, called the test functions: they generate our space Y_M. The weighted residuals minimization statement is then equivalent to the following variational formulation:

$$(3.3) \qquad \begin{cases} < \frac{\partial U_M}{\partial t} + L_M U_M - G_M, v >= 0 \quad \text{for all } v \in Y_M \\ U_M(x,0) = U_{0_M}(x) \end{cases}$$

where $< \cdot, \cdot >$ stands for the L^2 inner product on [0,1]. In the case of the Burgers equation (1), we will have $LU = -\nu \frac{\partial^2(U)}{\partial x^2}$, $G(U) = -\frac{1}{2}\frac{\partial(U^2)}{\partial x}$, $G_M(U) = \Pi_c(G(U)$ and the test functions θ_τ will be defined in the next paragraph.

3.1.3. Choice of the Test Functions and of the Time Discretization Scheme

The general idea of the algorithm is to comply with the localization of the wavelets in the Fourier space and in the physical space. We know that, in comparison to the Fourier functions e^{ikx}, the localization in the physical space implies the mixing of the frequencies that prevents the wavelets from being eigenfunctions of differential operators. However, they are not far from being so. Indeed, the localization of the wavelets in the Fourier space leaves the differential operators nearly diagonal.

In the particular case of the spline wavelets, it has been shown previously that, to a given precision α, the numerical supports of $\hat{\psi_{jk}}$ and $\hat{\psi_{j'l}}$ are disconnected as soon as $|j-j'| > n(\alpha)$ (for $\alpha = 10^{-3}, n = 1$). If D is a differential operator with constant coefficients, the same property holds also for $D\psi_{jk}$ and $\psi_{j'k}$ with a new precision α' depending on the spectrum of D. If, for instance $D = (1 - \nu\frac{\partial^2}{\partial x^2})$, the precision is unchanged.

The algorithm we are going to describe here takes large advantage of this property. Moreover, thanks to the fact that the coefficients of the Burgers equation are constant, some precalculations can be performed once and for all. Indeed, the main part of the work to be performed at each time step of the MWR can be done only one time and reused at every time step. This is done by a proper choice of the test functions θ_τ.

Let us be more precise in the case of an Euler time discretization scheme, implicit for the dissipation term and explicit for the convection term. This choice is made only for sake of simplicity in the following presentation and more sophisticated schemes are currently used for the numerical implementations (see Section 4).

Equation 3.3 is discretized as follows:

$$\begin{cases} < (1 - \nu\Delta t\frac{\partial^2}{\partial x^2})U_M^{n+1}, v >=< U_M^n - \frac{\Delta t}{2}\frac{\partial (U_M^n)^2}{\partial x}, v > \quad \text{for all } v \in Y_M \\ U_M(x,0) = U_{0_M}(x). \end{cases}$$

Choosing $\tau = (j,k)$ and $\theta_\tau = \theta_{jk}$ such that

$$\text{(3.5)} \qquad \begin{cases} \theta_{jk}(x) = \left(I - \nu\Delta t\frac{\partial^2}{\partial x^2}\right)^{-1}\psi_{jk}(x) \\ \theta_0(x) = \phi_{00}(x) \end{cases}$$

we invert once and for all the above direct problem at each scale.

Following this choice, the following set of equations is obtained:

$$\begin{cases} < U_M^{n+1}, \psi_{jk} >=< U_M^n, \theta_{jk} > + < -\frac{\Delta t}{2}\frac{\partial (U_M^n)^2}{\partial x}, \theta_{jk} > \\ < U_M^{n+1}, \phi_{00} >=< U_M^n, \theta_0 > \end{cases}$$

that can be written as:

$$(3.6)\qquad \begin{cases} < U_M^{n+1}, \psi_{jk} > = < U_M^n, \theta_{jk} > + < (U_M^n)^2, \theta'_{jk} > \\ < U_M^{n+1}, \phi_{00} > = < U_M^n, \theta_0 > \end{cases}$$

where we introduced another set of functions:

$$(3.7)\qquad \begin{cases} \theta'_{jk}(x) = -\frac{\Delta t}{2} \left(\frac{\partial}{\partial x} \left(I - \nu \Delta t \frac{\partial^2}{\partial x^2} \right) \right)^{-1} \psi_{jk}(x) \\ \theta'_0(x) = 0. \end{cases}$$

Using a Crank Nicholson discretization scheme and spline wavelets of order $m = 6$, the function θ associated with ψ_{up} using (3.5) is plotted on Figure 5. Roughly speaking, the θ_{jk} functions look like the corresponding wavelets ψ_{jk}: In the case of the spline wavelets, the θ_{jk} functions are exponentially localized in both Fourier and physical spaces. Moreover they have the same number of zero moments as the original wavelets and their numerical support in the Fourier space is included in those of the corresponding wavelets. At each scale, the θ_{jk} deduce one from the other by translation but the wavelet rescaling property from one scale to the other is no longer valid.

3.1.4. Computation of $< U_M^n, \theta_{jk} >$

A fast computation of these coefficients is possible thanks to the previous remarks. If, following 2.10, one writes:

$$\forall j \leq j_M - 2 \;\; \Pi_{V_{j_M}} = \Pi_{V_{j+2}} \oplus \sum_{j_M - 1 \geq l \geq j+2} \Pi_{W_l}$$

following 3.1.1 with $D = (1 - \nu \Delta t \frac{\partial^2}{\partial x^2})$, a numerically good approximation of $< U_M^n, \theta_{jk} >$ is $< \Pi_{V_{j+2}}(U_M^n), \theta_{jk} >$. Then, recalling that:

$$\Pi_{V_{j+2}} = \Pi_{V_{j+1}} \oplus \Pi_{W_{j+1}}$$

one gets

$$< U_M^n, \theta_{jk} > \simeq < \Pi_{V_{j+2}}(U_M^n), \theta_{jk} > \simeq < \Pi_{V_{j+1}}(U_M^n), \theta_{jk} > + < \Pi_{W_{j+1}}(U_M^n), \theta_{jk} > .$$

Since we have $\Pi_{V_{j+1}}(U_M^n) = \sum c_{j+1,\ell} \phi_{j+1,\ell}$ and $\Pi_{W_{j+1}}(U_M^n) = \sum d_{j+1,\ell} \psi_{j+1\ell}$ we obtain

$$< U_M^n, \theta_{jk} > \simeq \sum_{\ell} c_{j+1,\ell} \; \alpha_j(\ell - 2k) + d_{j+1,\ell} \beta_j(\ell - 2k)$$

where α_j and β_j are two families of discrete functions parameterized by j and depending on the multiresolution analysis, on the equation and on the time scheme. They are defined as

$$\forall n \in I\!N \;\; \alpha_j(n) = < \phi_{j,n}, \theta_{j-1,0} > \;\; \text{and} \;\; \beta_j(n) = < \psi_{j,n}, \theta_{j-1,0} >$$

and

$$\alpha(-n) = \alpha_j(n) \text{ and } \beta_j(-n) = \beta_j(n).$$

As in the tree algorithm (Section 2.3), the calculation of $\{< U_M^n, \theta_{jk} >, \; for \; 0 \leq j < j_{M-1} \; and \; 0 \leq k < 2^j\}$ involves two filtering procedures. The whole calculation requires order $N\text{Log}N$ operations. The coefficients of the filters α_j and β_j are stored in the memory at the beginning of the calculation in an array of size proportionnal to $N\text{Log}N$.

One wants to emphasize that the one-time computation involved in the calculation of the functions θ_{jk} is possible because the operator $I - \nu\Delta t\frac{\partial^2}{\partial x^2}$ has constant coefficients.

The computation of $< U_M^n, \theta'_{jk} >$ can be done the same way using two other families of filters, α'_j, β'_j, as soon as $(U_M^n)^2$ is computed (see next section).

Recalling that the filters $\alpha_j, \beta_j, \alpha'_j, \beta'_j$ depend on Δt, it must be said that the independence of Δt with respect to j is not required. Practically it means that the time step Δt can be adapted to the spatial scale, a possibility that can be useful in optimizing the time stability and precision conditions.

3.1.5. Estimation of the Nonlinear Terms

The calculation of the nonlinear terms, precisely $(U_M^n)^2$, is done using the classical collocation technique.

3.1.6. Implementation of the Algorithm

At each time step, the algorithm works as follows: supposing that (U_M^n) is known by its values at grid points, its scaling coefficients or its wavelets coefficients, U_M^{n+1} is computed using an order of $N\text{Log}N$ operations as shown in Table 1.

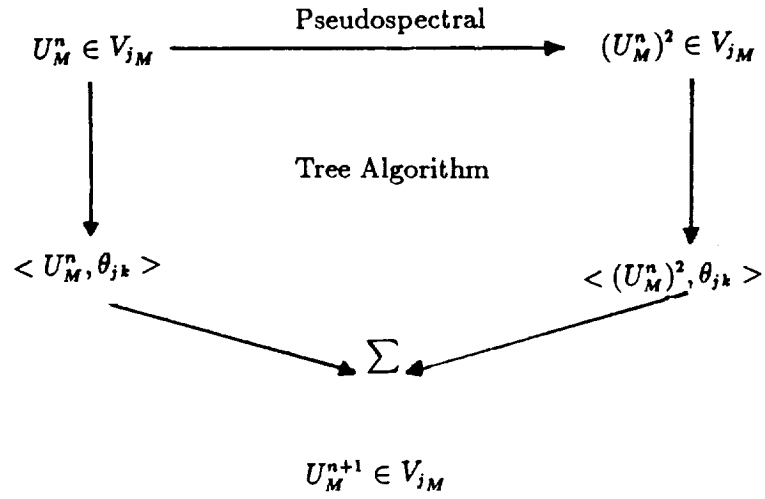

Table 1.

3.2. Description of the Algorithm on a Non Regular Grid

Up to now, X_M was equal to V_{j_M} which means that every wavelet ψ_{jk} with(j,k) such that $0 \leq j \leq j_M$ and $0 \leq k \leq 2^j - 1$ was considered in the approximation of the solution.

However, the distribution of scales significantly building a given function in the sense provided by its wavelet decomposition has no reason to be regular in the whole interval $[0,1]$. Figure 7 shows the wavelet decomposition of the solution of (1) as large gradient regions develop locally around $x = .5$. According to the values of the wavelet coefficients, small scales ($j \geq 5$) are only meaningful in a region very close to .5 and for time larger than $.5/\pi$. More precisely, if we choose a given precision α on the L^2 norm and look at the number of wavelets required to approximate the solution at different times it appears that only a small number of coefficients of the wavelet decomposition are needed. For instance, with a L^2 norm precision of 10^{-6} the number of wavelets required to reconstruct the solution at $t = 1/\pi$ is 74. The distribution of these "active" wavelets follows the cone shape structure of Figure 7. Our main goal is to compute only the wavelet coefficients $< U_M^n, \psi_{jk} >$ in a region as close as possible to this "active" space.

The adaptative version of our algorithm is designed in order to fulfill efficiently this requirement. It involves different steps:

Step 1: Estimation of the required space of approximation for the next time step: In a way comparable to what is done in spectral methods (see Gottlieb - Orzag 1977), the accuracy of the computation is examined, locally in the case of wavelets, from the shape of the local spectrum provided by the wavelet decomposition at every point.

Step 2: Adaptation of the space of approximation for the next time step: According to the result of the previous estimate and the knowledge of the operators of the Burgers equation, the space of approximation X_M is optimized (X_{M_a}) for future time by truncation of non "active" small scale wavelets or local addition of smaller scale wavelets (that are supposed to become "active" during the future time steps). (The smallest scale wavelets in X_{M_a} belong to $W_{j_{M_a}-1}$).

Step 3: Time advancing on the adapted space X_{M_a}.

We are going now to describe in more detail the adaptative version of the algorithm in terms of flagging criterion (Step 1) and new trial and test functions (Steps 2 and 3). Moreover it will be shown that the general structure of the algorithm remains unchanged.

3.2.1. New Trial Space X_M and Test Space Y_M but Same Algorithm

Figure 4 shows the selected values of (j,k) of an adapted grid generated by the adapted

version of the algorithm for the Burgers equation (1) at $t = 1/\pi$. Precisely,

$$X_{M_a} = \text{ span } \{\psi_{jk}, (j,k) \in JK\}$$

where

$$JK = \{(j,k) \text{ such that } 0 \leq j < j_M, 0 \leq k < 2^j$$

$$\text{or such that } j = j_M, k_1 \leq k \leq k_2$$

$$\text{or, } j = j_M + 1, k_1' \leq k \leq k_2'\}$$

with $j_M = 6, k_1 = 22 \;\; k_2 = 31 \;\; k_1' = 54 \;\; k_2' = 73. \;\; j_{M_a} = 8.$

To define completely the algorithm, one has also to define the Y_{M_a} space. This is done in exactly the same way as it has been presented in the regular case: the generating functions of Y_{M_a} are derived from the basis functions of X_{Ma} using (3.5). Due to the local form of the algorithm, the whole procedure remains unchanged when the trial and test spaces are adapted. The complete procedure is identically reproduced without modification.

This highly attractive property is due to the localization properties of the wavelets and of the algorithm in physical and Fourier spaces.

The adaptive procedure is precisely a controlled modification of the space of approximation in which one looks for the solution. As this procedure consists in adding or subtracting orthonormal functions, the so-called restriction and interpolation operators are exactly known: they are directly provided by the tree algorithm. Moreover, no reversibility problems are encountered during the restriction and interpolation procedures.

For completeness, some words must be said on the flagging procedure used to modify the subscript space JK (this is the practical way to adapt X_M). In the case of the Burgers equation, this procedure is very simple and cheap. Basically, starting from the smallest scale available (j_{SS}),the attention is focused on the smallest scale projection of the solution

$$\Pi_{W_{jss}}(U_M^n) = \sum_{k \text{ such that } (j_{SS},k) \in JK} < U_M^n, \psi_{jss,k} > \psi_{jss,k}.$$

As shown in Section 2 and Figure 8, this function is localized in the strong gradient regions. The energy associated with the wavelets ψ_{jssk}, precisely $| < \psi_{jss,k}, U_M^n > |^2$, reveals the amount of energy of the solution in the scale j_{SS} around the point $\frac{1}{2^{j_{SS}+1}} + \frac{k}{2^{j_{SS}}}$. The Burgers equation is such that, due to the presence of nonlinear terms in the equation that generate smaller and smaller scale, only small values of these coefficients are relevant (otherwise oscillations occur). Consequently, if $| < \psi_{jssk}, U_M^n > |^2$ is greater than a predetermined value, the space X_M of approximation is adapted by adding new smaller scaled wavelets $\psi_{j_a l}$, $(j_a = j_{SS} + 1)$, around the point $\frac{1}{2^{j_{SS}+1}} + \frac{k}{2^{j_{SS}}}$. Adaptivity means also

restriction of the space X_{M_a} and, using a comparable criterion, small scale (j_{SS}) wavelets can be removed in a region where the terms $| < U_M^n, \psi_{j_{SS}\ell}|^2$ are not significant. (This occurs in the second regime of the Burgers solution when the viscosity smooths the gradients previously generated during the first regime.)

4. NUMERICAL RESULTS

This section is devoted to a practical and numerical description of the algorithm. The basic elements of the problem and the algorithm are repeated for clarity.

The periodic regularized Burgers equation

$$\begin{cases} \frac{\partial U}{\partial t} + \frac{U \partial U}{\partial x} = \frac{\nu \partial^2 U}{\partial x^2} \\ t \geq 0, x \in [0,1], \nu = \frac{10^{-2}}{\pi} \\ U(0,t) = U(1,t) \\ U(x,0) = \sin(2\pi x) \end{cases}$$

is solved numerically in the space of splines of order $m = 6$. The trial functions are the periodic spline wavelets ψ_{jk} and ϕ_{00} . The test functions are defined following the general procedure described in Section 3.1.5. All the following results are obtained using an Adams-Bashforth time scheme for the nonlinear convection term and a Crank-Nicholson time scheme for the diffusion term. The integration time step, for every scale is $\Delta t = 10^{-3}$. We recall here, that the choice of the time scheme and the value of Δt directly influence the definition of the functions θ_{jk} and θ'_{jk}. However, knowing the time discretization scheme, their estimation is staightforward.

The filters used in the wavelet decomposition are noted h and g. The filters defined to compute the scalar products $< U_M^n, \theta_{jk} >$ and $< (U_M^n)^2, \theta'_{jk} >$ are noted α_j, β_j and α'_j, β'_j respectively. The Figures 1, 2, and 5 show in the Fourier and in the physical spaces some selected elements of the different mathematical beings defined above.

The evolution of the approximated solution $U(x,t)$ from $t = 0$ to $t = \frac{1.5}{\pi}$ is plotted on Figure 6 where $j_M = 8$ and a regular grid (Figure 3) is used. Considering the theoretical solution of the Burgers equation (see [Basdevant et al. 1986]), this can be considered as a reference estimation of the solution. Figure 7 shows the wavelet coefficients of the solution at the same times. Figure 8 shows the time evolution of the energy carried by the scale $j = 6$.

At the same times, the same elements are plotted for a calculation run using $j_M = 7$ and a regular grid. Figure 9 reveals that the lack of resolution in the strong gradient region (around $x = .5$) induces numerical oscillations of the solutions close to those observed

when a Gibbs phenomenon occurs. These oscillations are however localized in space mainly thanks to the filtering operation performed by the spline projection of the variables and their derivatives. Figure 10 shows again the time evolution of an approximate solution obtained with a computation started with $j_M = 6$ (that is to say $2^6 = 64$ degrees of freedom and $j_{SS} = 5$) and that has been obtained using the adaptative procedure. From a time close to $t_a = .5/\pi$ when the local gradients begin to be very large the adaptative procedure adapts progressively the space to $j_{M_a} = 7$ and $(k_1, k_2) = (22, 31)$ (that is to say $64 + 20 = 84$ degrees of freedom) and then (for $.66/\pi \leq t \leq 1.4/\pi$) to $j_{M_a} = 8$ and $(k_1', k_2') = (54, 73)$ (that is to say $64 + 20 + 20 = 104$ functions). The corresponding dyadic grid is the one of Figure 4, the smallest scales $j = 6$ and $j = 7$ being used only when required. Finally on Figure 11, the evolution of the approximate solution using the same time discretization and a Fourier pseudospectral spatial discretization is plotted. The resolution is $2^7 = 128$. First, one observes, in comparison to Figure 9 which is obtained with the same resolution (i.e the same number of degrees of freedom), that the oscillations are much more spread in the Fourier case, due to the non localization of the basis. Secondly, comparison with Figure 10 shows that with a maximum of 104 well distributed degrees of freedom, a much better result can be obtain from the adapted algorithm. It is known (see [Basdevant et al. 1986]) that to improve the precision of a Fourier spectral method without increasing the number of degrees of freedom, intricate coordinate transformations are required that imply moreover an a priori knowledge of the solution shape.

A comparison of the four different approximations presented above is made in Table 2. $T_{\max}$ is the time needed to reach the maximum slope at $x = 0.5$, and $S_{\max}$ is the value of this slope. No optimization study of the time marching scheme has been made that would have improved the estimates of $S_{\max}$ and $T_{\max}$ (see [Basdevant et al. 1986]).

Table 2: Comparison of some different methods.

Algorithm (AB-CN Time scheme)	$2\pi T_{\max}$ Exact:1.6037	$S_{\max}/2.$ Exact:152.005		Degrees of freedom
Present Algorithm. $m = 6$ $j_M = 8$, regular grid	1.64	150.3	No oscillations	256
Present Algorithm. $m = 6$ $j_M = 7$, regular grid	1.63	135.0	Localized oscillations	128
Present Algorithm. $m = 6$ $j_M = 6, j_{M_a} = 8$ adapted grid	1.64	150.3	No oscillations	≤ 104
Fourier pseudospectral $n = 128$	1.62	134.8	Spread oscillations	128

5. CONCLUSIONS

The numerical resolution of the 1D periodic and regularized Burgers equation has been performed using a new algorithm. This algorithm is based on the wavelet representation of the space of approximation. In the so-called regular grid case, this space is nothing more than the classical spline space, but in the non regular grid case it is more flexible than a classical grid refinement generated space.

The special feature of this algorithm that uses explicitly the wavelet basis stands on the fact that it extensively takes into account the localization properties of the wavelets in the physical and Fourier spaces. Indeed, the exponential decay of the spline wavelets in both spaces allows, on one hand handling the differential operators as if they were nearly diagonal and, on the other hand, working in the physical space with very flexible orthogonal and numerically well localized functions. The scale decomposition provided by the wavelet coefficients and the knowledge of the Burgers operators are used to manage at each time step the space of approximation. The whole algorithm can then adapt itself to the solution. Moreover, in the case of constant regular operators, advantage can be taken by pre-inverting the problem at each scale once and for all at the beginning of the calculation. Then, the whole algorithm can be seen as a time advancing pyramidal algorithm.

In this paper, the method has been described and a numerical application has been provided that uses spline wavelets of order 6. Some mathematical remarks have been given but the results on numerical analysis of the method will be published elsewhere.

To date, we are not sure that the choice of the spline wavelets is optimal for efficient and adaptable resolution of partial differential equations; furthermore, the existence of a stronger connection between the wavelets and the resolved equation at each scale has not been investigated. However, it must be recalled that the spline wavelets achieve an optimal combined localization in physical and Fourier spaces, as far as orthonormal wavelets are concerned.

The limitation to a 1-D problem and periodic boundary conditions is not connected to the algorithm or the wavelet approach even if various specific problems will have to be faced. This choice has been made for clarity and simplicity. Extensions to more realistic problems involving different boundary conditions and multidimensions are currently underway.

REFERENCES

C. Basdevant, M. Deville, P. Haldenwang, J. M. Lacroix, J. Ouazzani, and R. Peyret: "Spectral and finite difference solution of the Burgers equation," Computers and Fluids, Vol. 14, No. 1, pp. 23-41 (1986).

G. Battle: "A block spin construction of ondelettes, Part I: Lemarié functions," Commun. Math. Phys. 110, 601-615 (1987).

C. Canuto, M. Y. Hussaini, A. Quarteroni, and T. A. Zang: "Spectral methods in fluid dynamics," Springer Series in Computational Physics (1987).

D. Gottlieb and S. Orszag: "Numerical analysis of spectral methods: Theory and applications," SIAM-CBMS Philadelphia (1977).

P. G. Lemarié: "Ondelettes à localisation exponentielles," Journ. de Math. Pures et Appl. 1989.

S. Mallat: "Multiresolution representations and wavelets," Ph.D., MS-CIS-88-68, Grasp Lab 153, University of Pennsylvania, Philadelphia, PA 19104 (1988).

S. Mallat: "A characterization of signals from the wavelet transform maxima," NSF/CBMS Conference on Wavelets, Lowell University (1990).

Y. Meyer: "Ondelettes et Opérateurs 1: Ondelettes," Herman (1990).

V. Perrier and C. Basdevant: "La décomposition en ondelettes périodiques, un outil pour l'analyse de champs inhomogénes. Théorie et algorithmes," la Recherche Aérospatiale, No. 3, pp. 53-67 (1989).

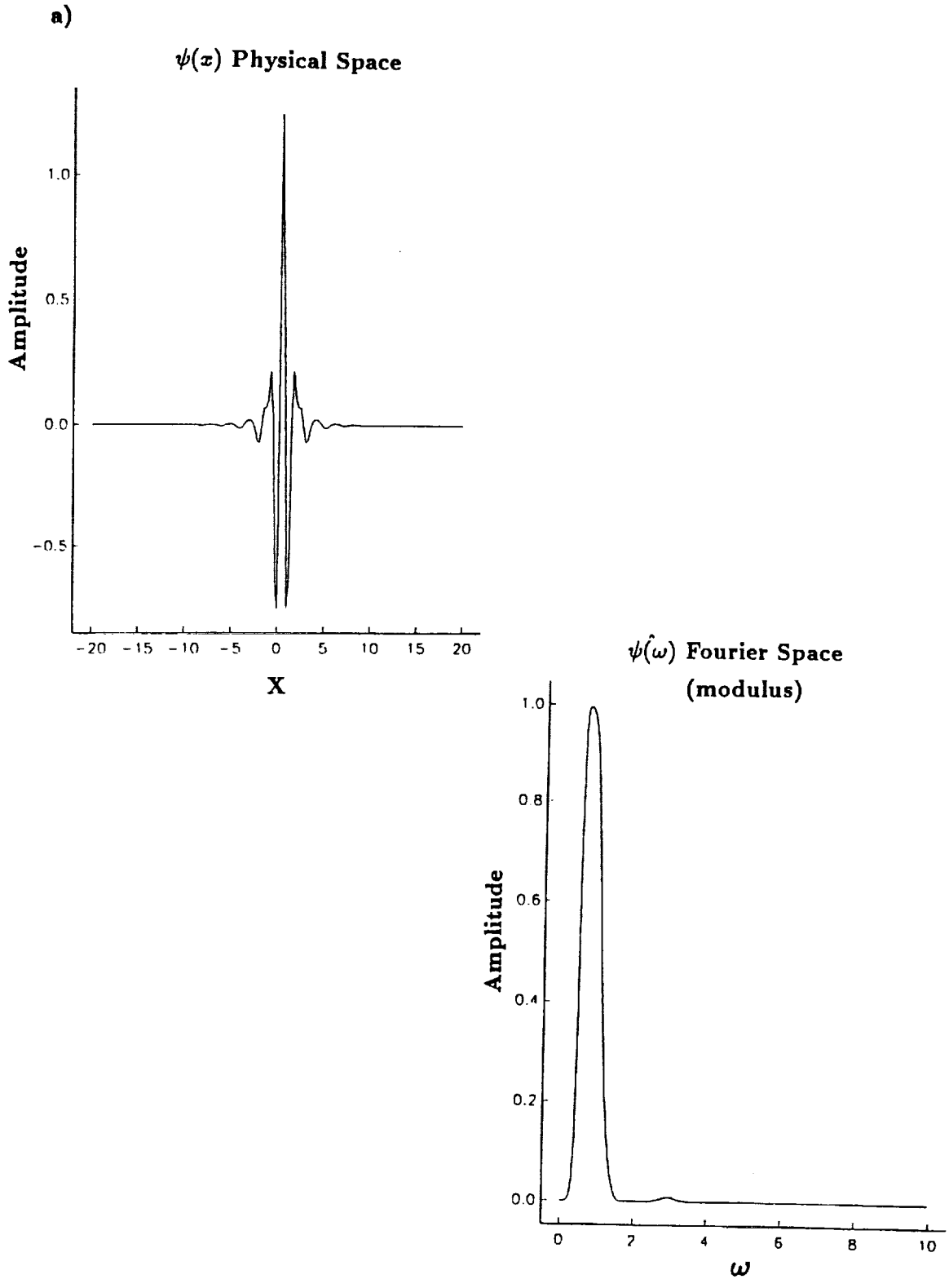

Figure 1. a) Spline wavelets for $m = 6$ in physical and Fourier spaces. b) Spline scaling functions for $m = 6$ in physical and Fourier spaces.

b)

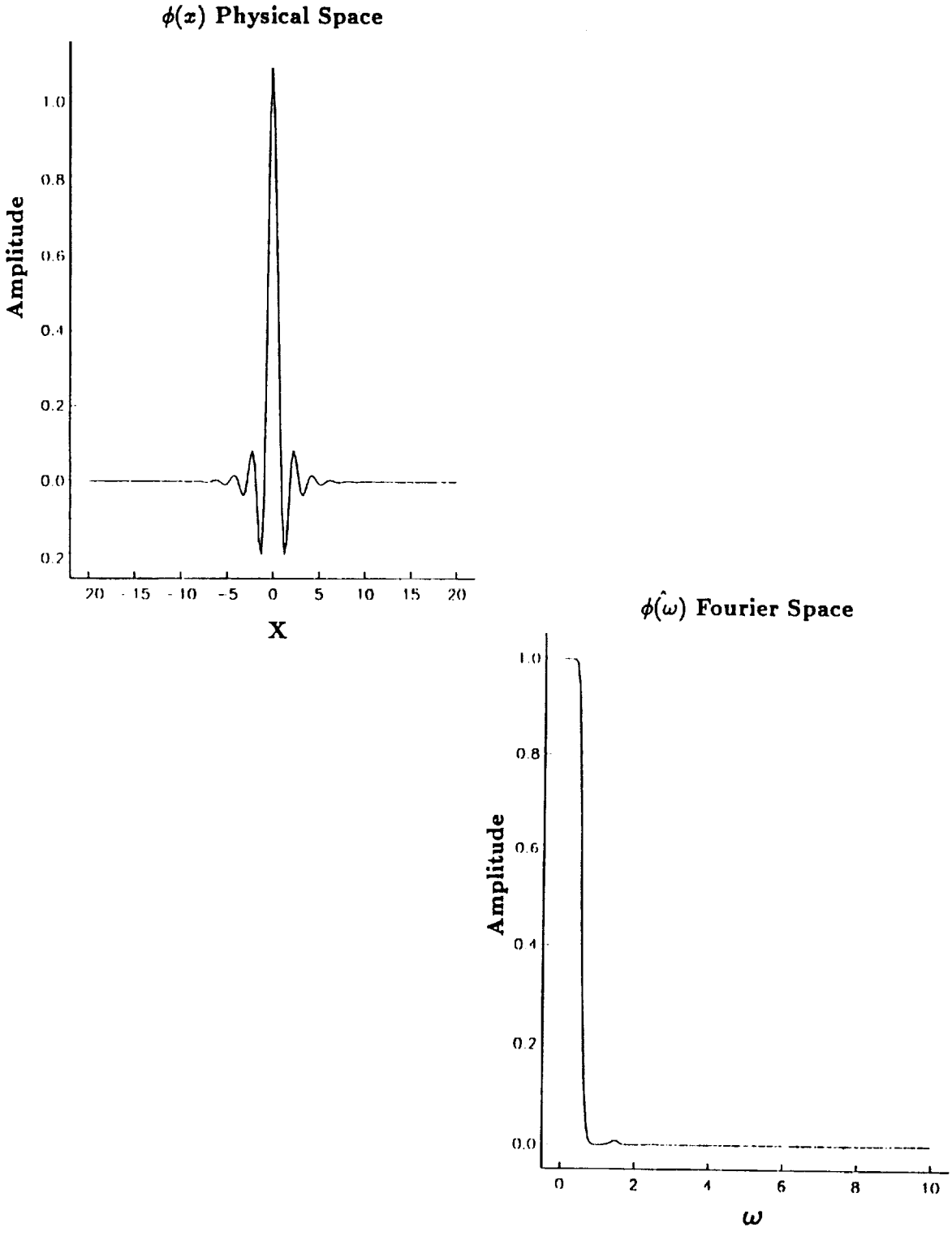

Figure 1. **(Continued)**

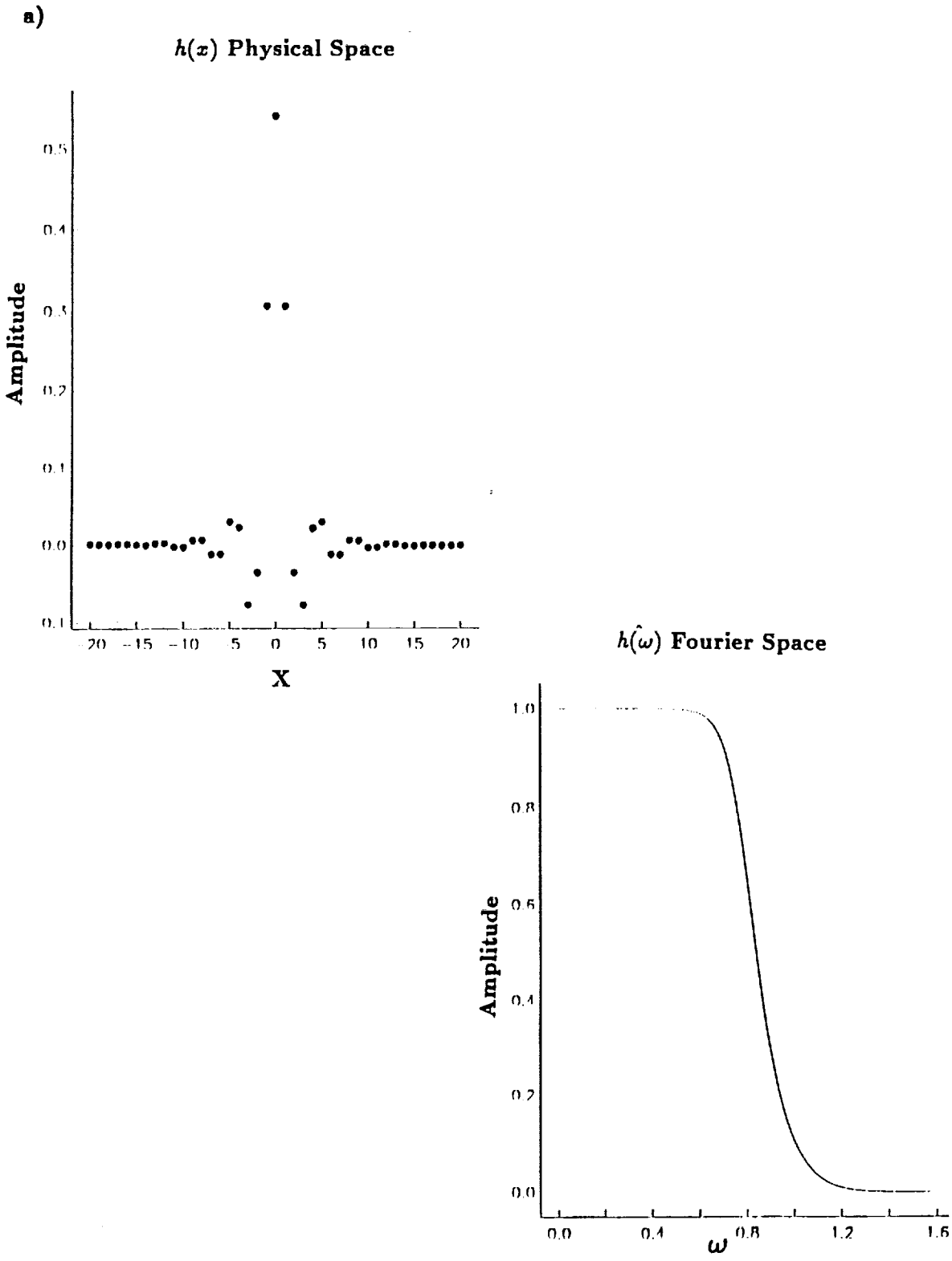

Figure 2. **a) h function, for the $m = 6$ spline multiresolution analysis, in physical and Fourier spaces.**
b) g function, for the $m = 6$ spline multiresolution analysis, in physical and Fourier spaces.

b)

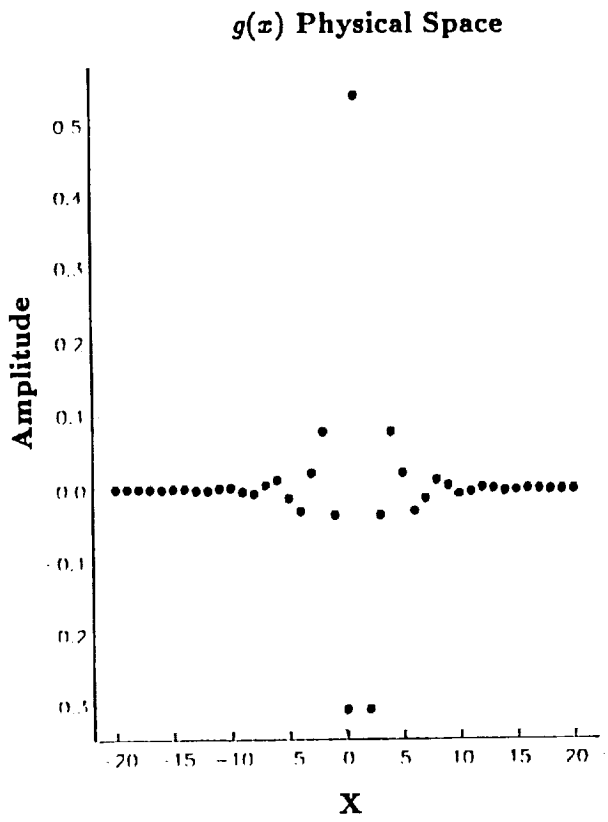

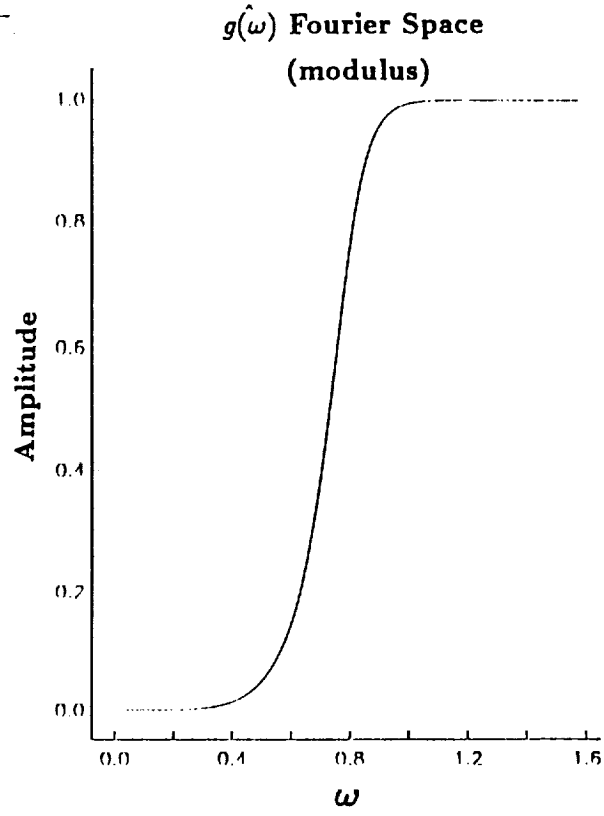

Figure 2. (Continued)

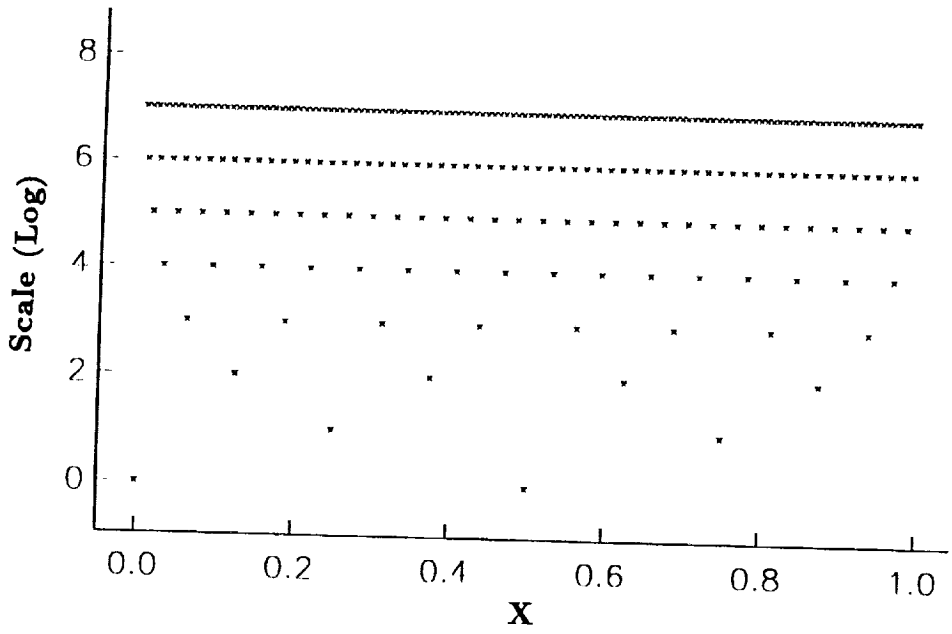

Figure 3. **Regular dyadic grid (centers of $\psi_{jk}, 0 \leq j < j_M, 0 \leq k < 2^j$ and of $\phi_{0,0}$) ($j_M = 8$).**

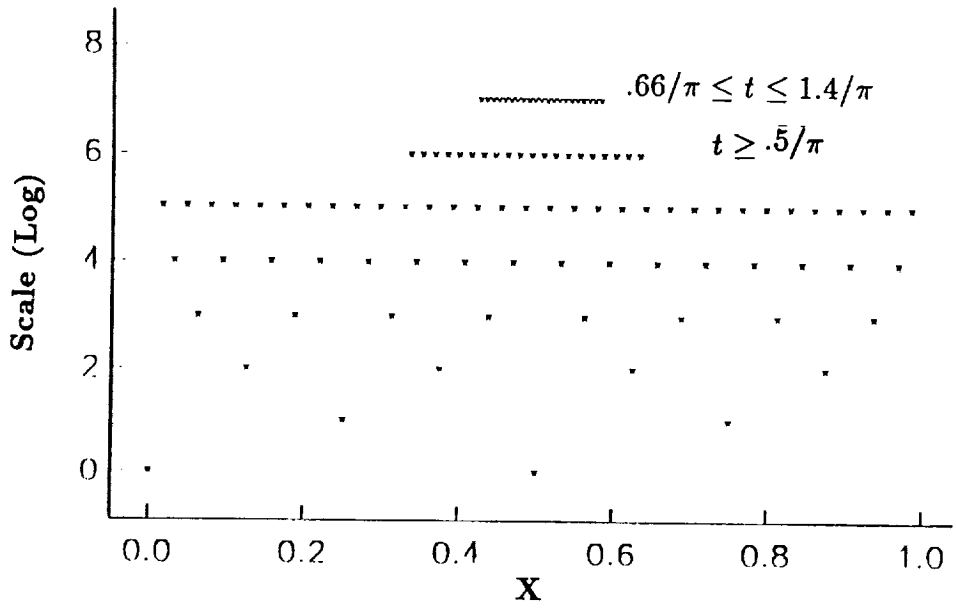

Figure 4. **Adapted dyadic grid $j_M = 6$,$\{j = 6, k_1 = 22, k_2 = 31\}$,$\{j = 7, k_1' = 54, k_2' = 73\}$.**

a)

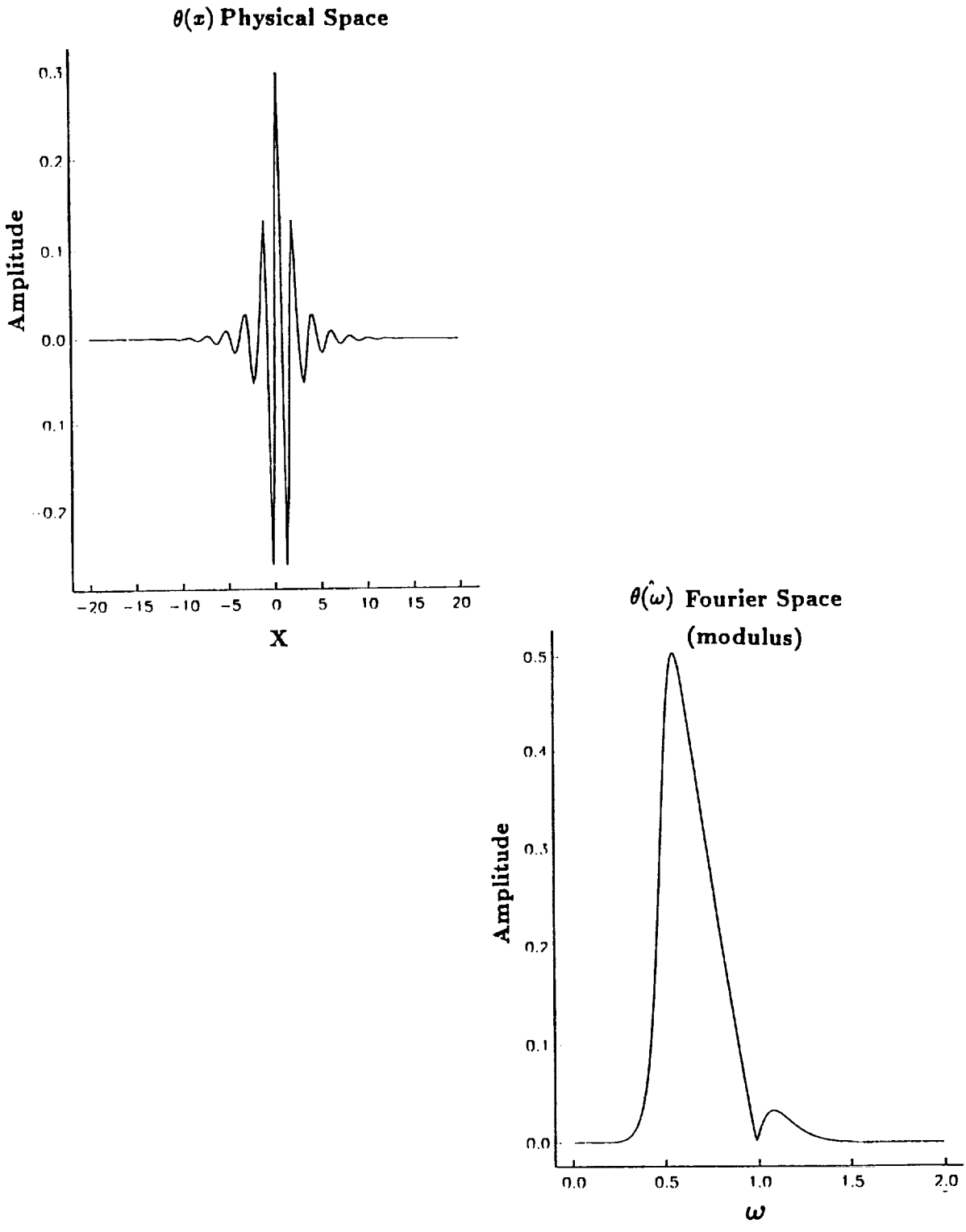

Figure 5. a) θ *for* $m = 6$, in physical and Fourier spaces.
b) α_j, β_j, $m = 6, j = 7$ in physical and Fourier spaces.

b)

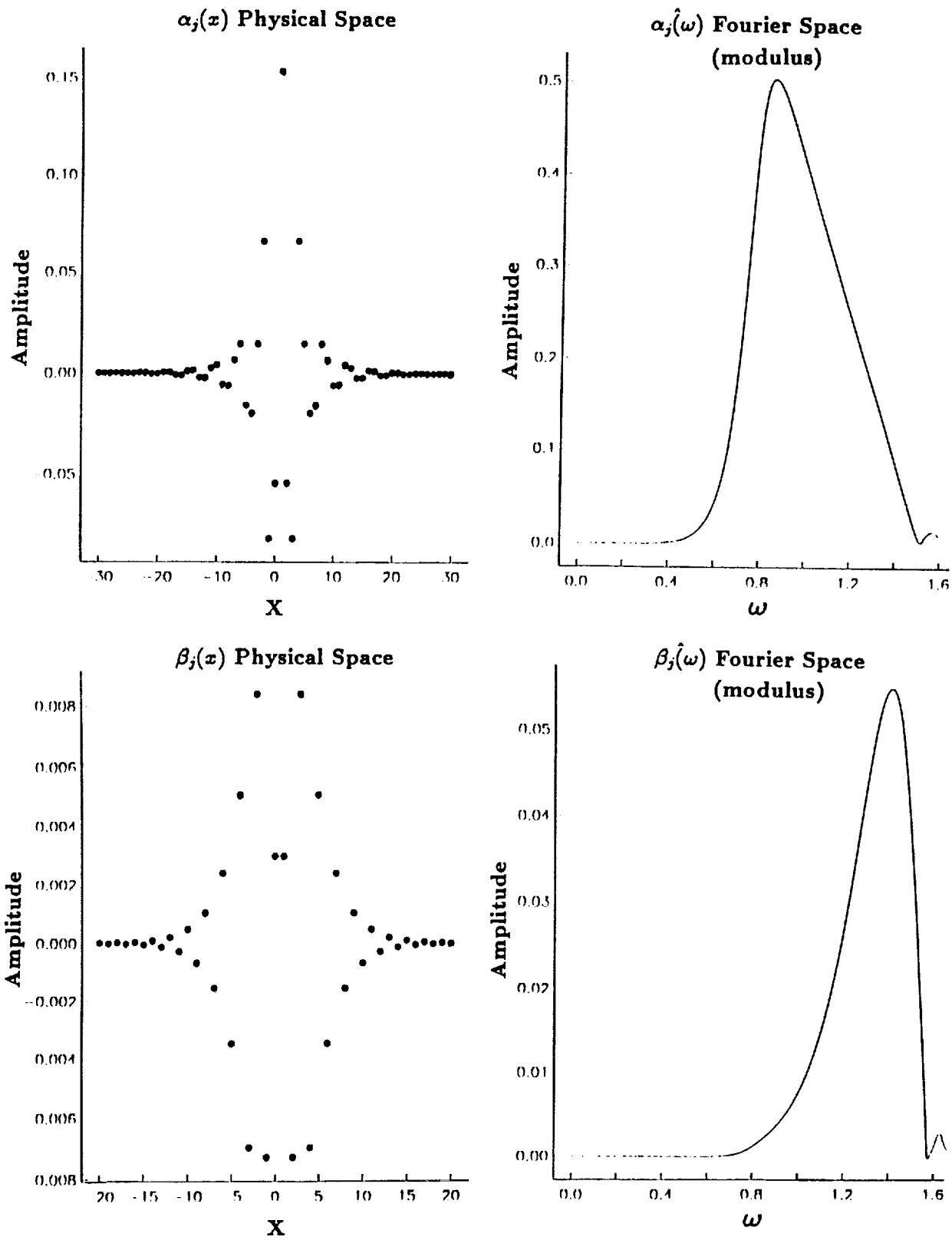

Figure 5. (Continued)

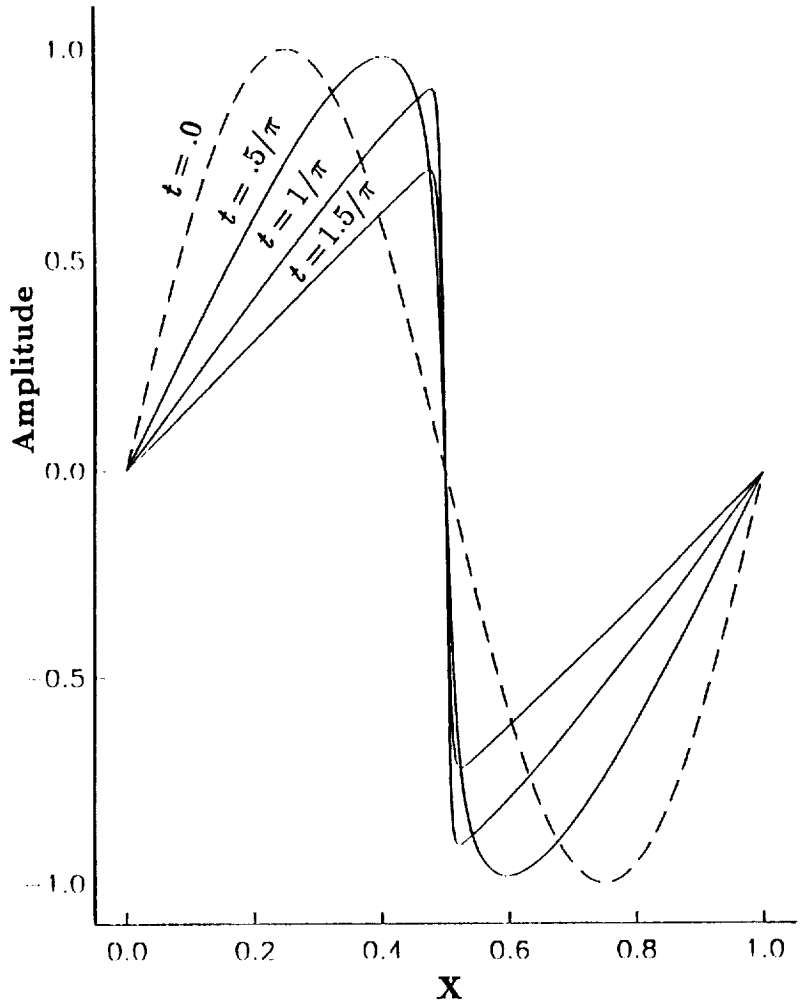

Figure 6. **Time evolution of the approximated solution: $m = 6, j_M = 8$ regular grid algorithm. 256 degrees of freedom.**

Figure 7. Time evolution of the wavelet coefficients of the approximated solution $m = 6, j_M = 8$, regular grid. For each value (j,k) of JK, a rectangle of length 2^{-j} and width 1 centered around $x = \frac{1}{2^{j+1}} + \frac{k}{2^j}$ and $y = j$ is plotted with a constant grey level connected to the absolute value of the (j,k) wavelet coefficient.

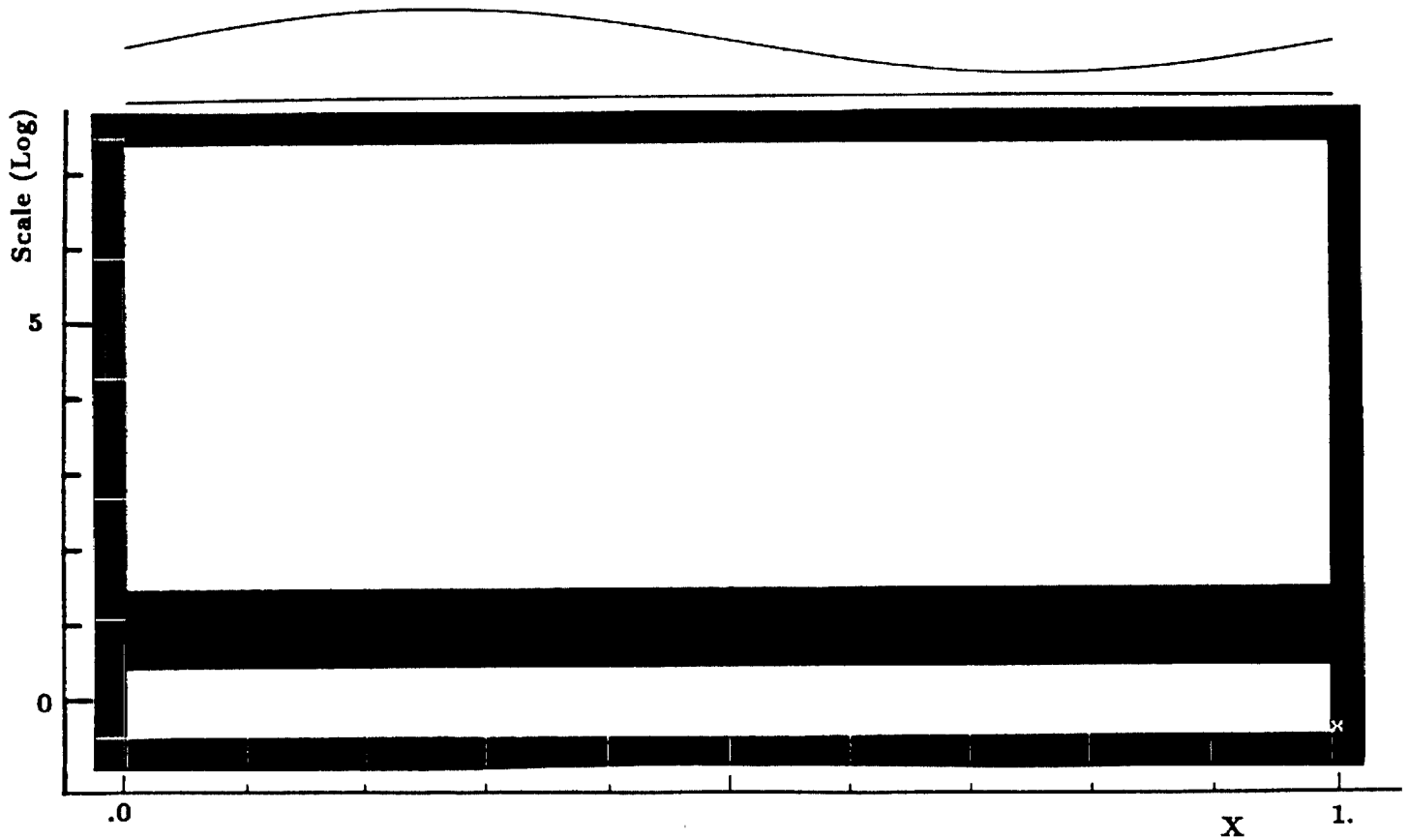

Figure 7. (Continued)

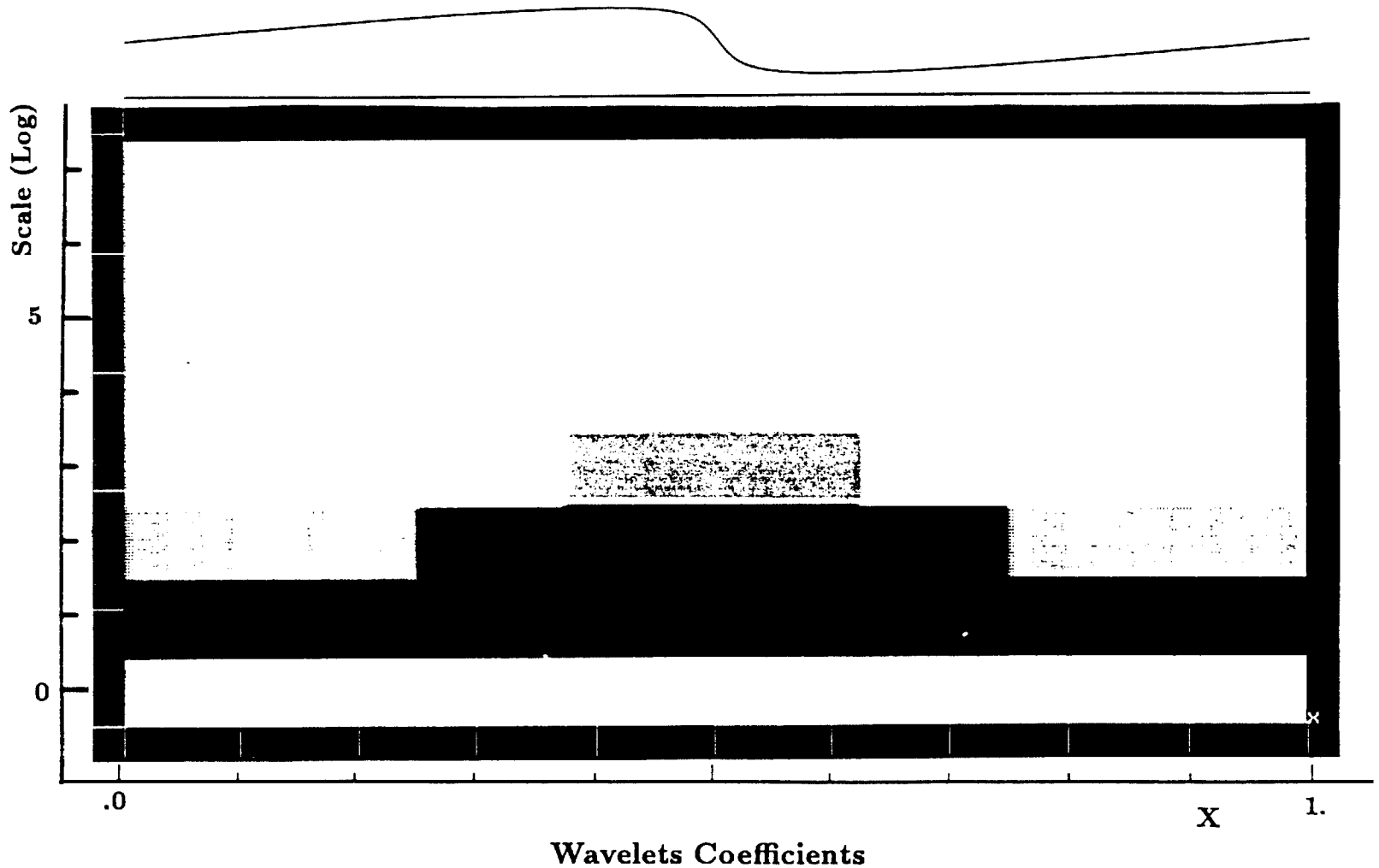

Wavelets Coefficients

of the Approximated Solution 256 degrees of freedom

$t = .5/\pi$

Figure 7. (Continued)

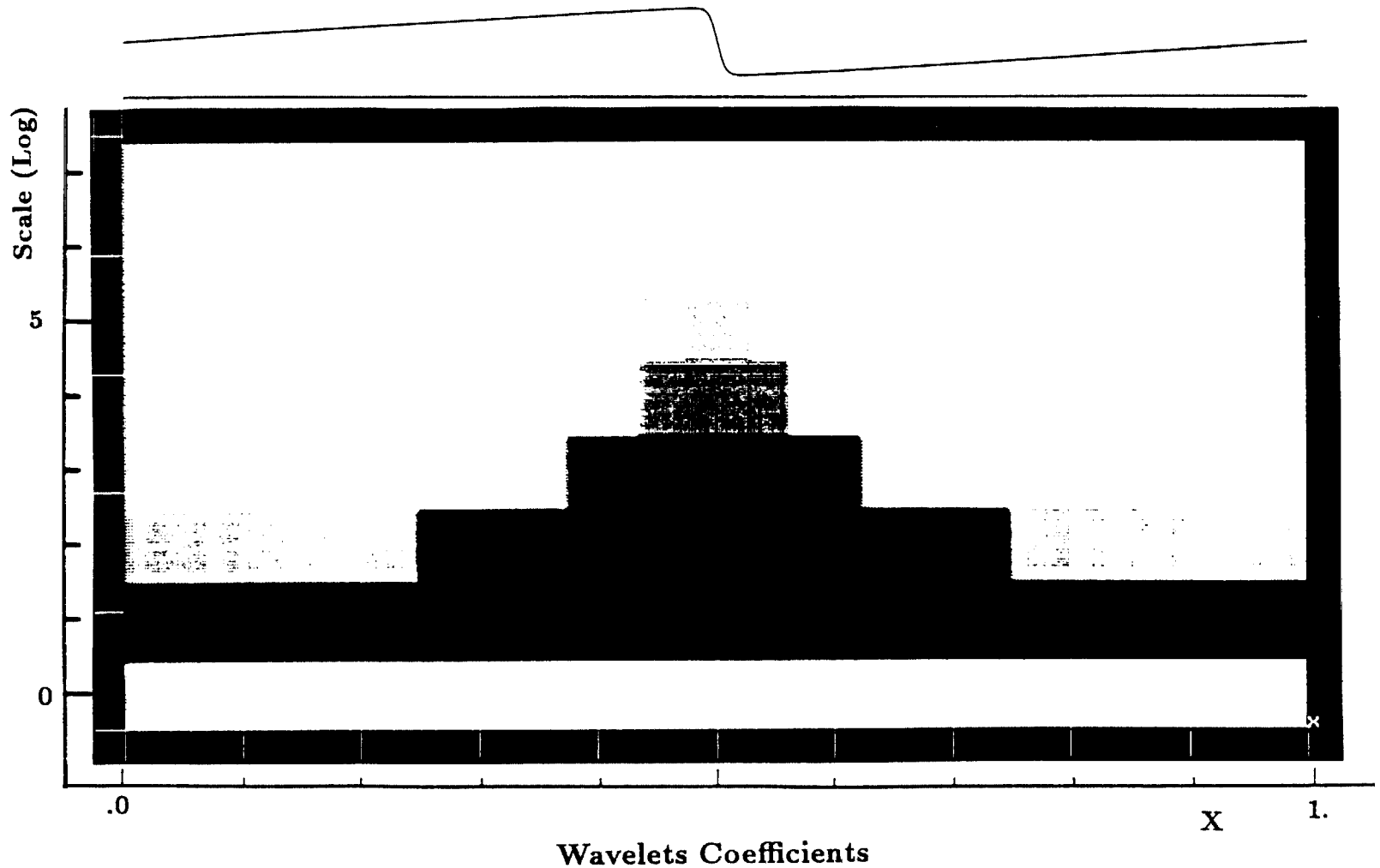

of the Approximated Solution 256 degrees of freedom

$t = 1/\pi$

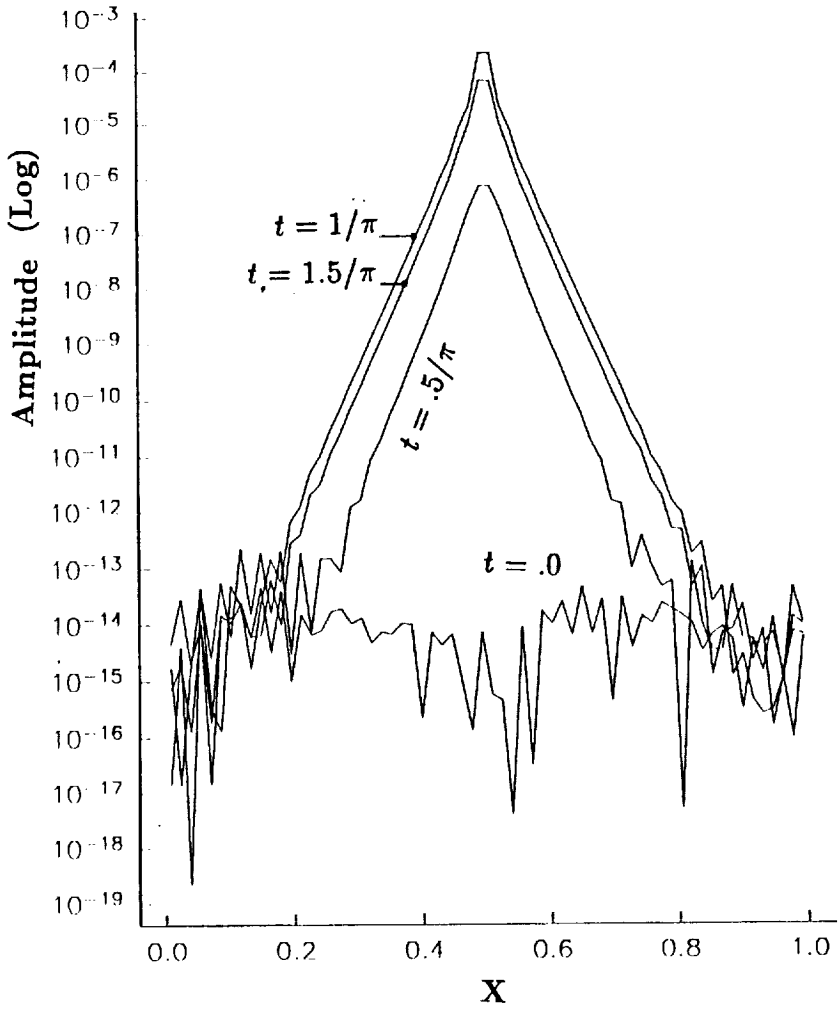

Figure 8. **Time evolution of small scale ($j = 6$) energy.**

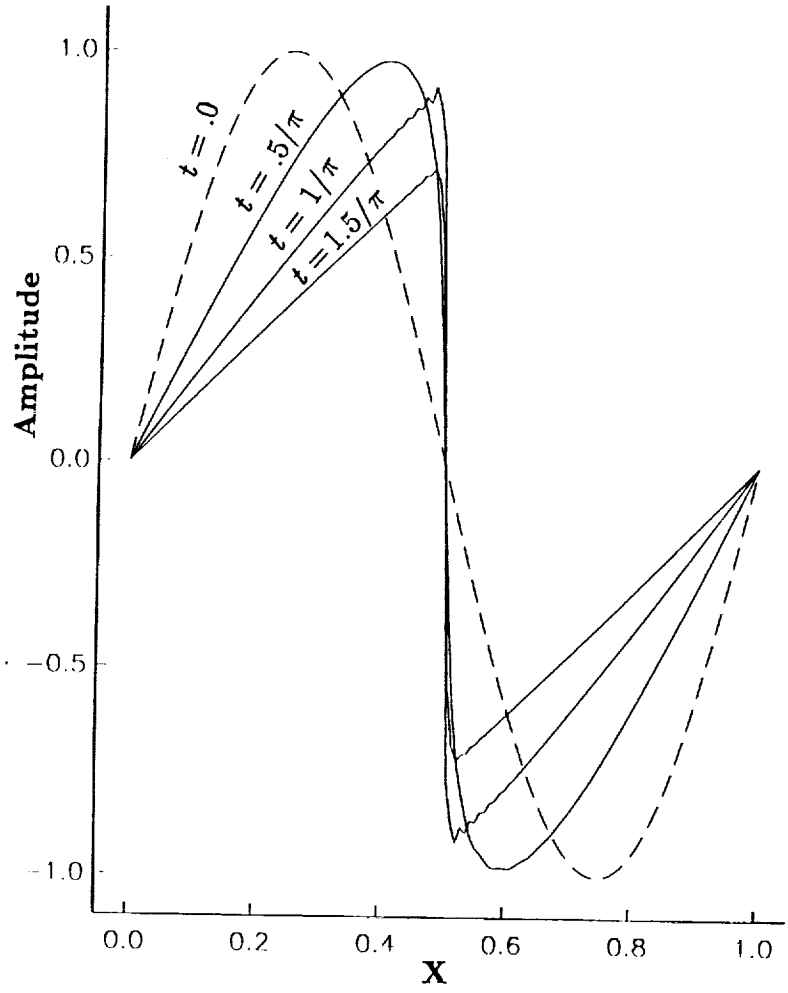

Figure 9. **Time evolution of the approximated solution $m = 6, j_M = 7$ regular grid algorithm. 128 degrees of freedom.**

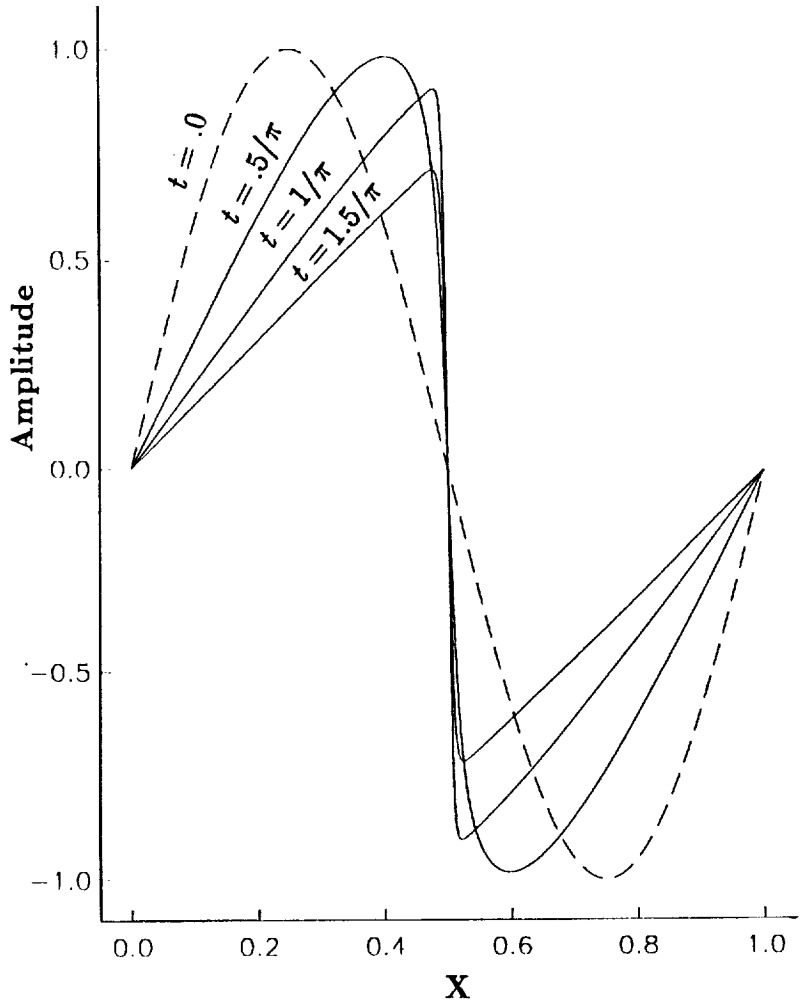

Figure 10. **Time evolution of the approximated solution $m = 6, j_M = 6, j_{Ma} = 7$, adapted algorithm . The maximum number of degrees of freedom during the whole computation is 104.**

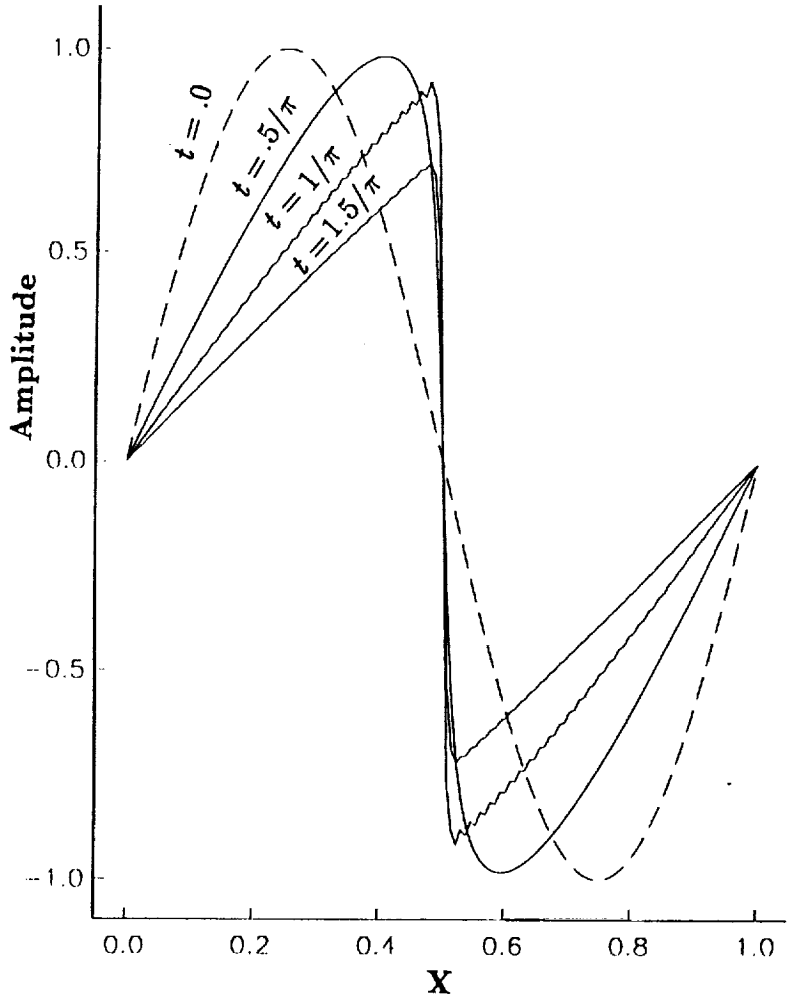

Figure 11. **Time evolution of a Fourier pseudospectral solution, resolution = 128.**

NASA
National Aeronautics and Space Administration

Report Documentation Page

1. Report No.	2. Government Accession No.	3. Recipient's Catalog No.
NASA CR-187480 ICASE Report No. 90-83		

4. Title and Subtitle	5. Report Date
RESOLUTION OF THE 1D REGULARIZED BURGERS EQUATION USING A SPATIAL WAVELET APPROXIMATION	December 1990
	6. Performing Organization Code

7. Author(s)	8. Performing Organization Report No.
J. Liandrat Ph. Tchamitchian	90-83
	10. Work Unit No.
	505-90-21-01

9. Performing Organization Name and Address	11. Contract or Grant No.
Institute for Computer Applications in Science and Engineering Mail Stop 132C, NASA Langley Research Center Hampton, VA 23665-5225	NAS1-18605
	13. Type of Report and Period Covered
	Contractor Report

12. Sponsoring Agency Name and Address	14. Sponsoring Agency Code
National Aeronautics and Space Administration Langley Research Center Hampton, VA 23665-5225	

15. Supplementary Notes

Langley Technical Monitor:
Richard W. Barnwell

Submitted to Annales Institut Henri Poincaré

Final Report

16. Abstract

The Burgers equation with a small viscosity term, initial and periodic boundary conditions is resolved using a spatial approximation constructed from an orthonormal basis of wavelets.

The algorithm is directly derived from the notions of multiresolution analysis and tree algorithms. Before the numerical algorithm is described these notions are first recalled. The method uses extensively the localization properties of the wavelets in the physical and Fourier spaces. Moreover, we take advantage of the fact that the involved linear operators have constant coefficients. Finally, the algorithm can be considered as a time marching version of the tree algorithm.

The most important point is that an adaptive version of the algorithm exists: it allows one to reduce in a significant way the number of degrees of freedom required for a good computation of the solution.

Numerical results and description of the different elements of the algorithm are provided in combination with different mathematical comments on the method and some comparison with more classical numerical algorithms.

17. Key Words (Suggested by Author(s))	18. Distribution Statement
wavelet approximation, numerical method, P.D.E.	64 - Numerical Analysis Unclassified - Unlimited

19. Security Classif. (of this report)	20. Security Classif. (of this page)	21. No. of pages	22. Price
Unclassified	Unclassified	36	A03

NASA FORM 1626 OCT 86